

Effects of diesel-ethanol-waste oil cooking and plastics blends reused in common rail direct injection diesel engine

D.V.S.R.B.M. Subrahmanyam, Manikandan Jegathesan

Department of Mechanical Engineering, Annamalai University, Annamalainagar, India

Article Info

Article history:

Received Jun 27, 2023

Revised Jul 23, 2023

Accepted Aug 15, 2023

Keywords:

Diesel engine

Ethanol

Nox emissions

Plastic oil

Smoke emission

Thermal efficiency

Waste energy reuse

ABSTRACT

The purpose of this study was to investigate the feasibility of transesterifying waste oils using alcohol and a catalyst to provide a sustainable fuel alternative. To ensure that the resulting biodiesel met American Society for Testing and Materials (ASTM) criteria, we studied its most important parameters of diesel-ethanol-waste oil cooking and plastics blends. We were able to separate out three unique fuel mixtures: BF0 (100% diesel), E20 (20% ethanol and 80% diesel), W20 (20% waste cooking oil and 80% diesel), and P20 (20% waste plastics oil and 80% diesel). In this experiment, a single-cylinder, computer-controlled diesel engine with direct injection was used. Fuel consumption increased by 4.3% for W20, 6.7% for E20, and 0.4% for P20, while thermal efficiency decreased by 2.1% for W20, 4.2% for P20, and 2.1% for E20, based on measurements conducted at 23.5 °b top dead center (TDC), compression ratio (CR19) under full load. At 23.5 °b TDC injection time, NOx emissions were observed to be lower. Adding 20% W to conventional fuel at 23.5 °b TDC enhanced the engines combustion characteristics.

This is an open access article under the [CC BY-SA](https://creativecommons.org/licenses/by-sa/4.0/) license.



Corresponding Author:

D.V.S.R.B.M. Subrahmanyam

Department of Mechanical Engineering, Annamalai University

Annamalainagar, 608002, Tamil Nadu, India

Email: subhramanyasharma@gmail.com

1. INTRODUCTION

The usage of energy all around the world is always going up. Because of their limited supply and detrimental effects on the environment [1], [2], it is no longer an option to depend on fossil fuel-derived energy or petroleum to power our homes and businesses. In addition, energy sources based on fossil fuels produce a great deal of pollution and contribute to the intensification of carbon emissions, both of which contribute to global warming and ozone depletion. As a result of this, there has been a growing desire for alternative sources that are based on renewable resources for applications in the real world [3], [4]. Biomass is the most robust and resilient of the renewable energy sources now accessible, and its consequences are far less severe than those of fossil fuels. In addition, it is the most common since it is responsible for eighty percent of the renewable energy that is created all over the globe, particularly for the purposes of transportation, heating, and power generating. Ethanol (E) use has increased recently [5], [6], waste cooking oil (W) [7], [8], and plastics oil (P) [9], [10] to make compression ignition (CI) engine fuels. This is due to the fact that it is regarded as the disposal method that generates the least amount of pollution for 'W' and because it promotes energy variety and circular bio-economy.

The impact of pine oil biofuel combined with base fuel of diesel at change in injection parameter and loads for P30 mixture has been explored by [11]. Chen *et al.* [11] discovered that increasing the injection pressure led to an increase in brake thermal efficiency (BTE) levels. The greatest BTE that can be reached with P30 fuel is 26.1% when it is compressed to 350 pressure, which is 6.9% more than the BTE that can be achieved

with diesel when compressed to 200 bar. Because of the increased atomization of the fuel, the quicker evaporation, and the production of the better air fuel combination, the exhaust emissions of hydrocarbons (HC), carbon monoxide (CO) and smoke steadily reduced as the fuel injection pressure was raised. The P30 blend reduces CO and HC emissions by 16.6% and 13.1% at 300 bar compared to pure diesel at 200 bar. This decrease occurs at 100% load state. When compared to that of diesel at 200 pressure, the NO_x produced by P30 mix at 350 bar is about 9.4% more than that produced by diesel. Han *et al.* [12] show how the spray properties and atomization of the fuel are affected by the injection pressure at 180-240 MPa, respectively. The engine's characteristics are improved by 240 MPa when the injection pressure is set to its optimal level. At an injection pressure of 240 MPa, the B30 demonstrated much lower emissions than both the B10 and the B20. Wang *et al.* [13] describes the influence of injection pressure (four bars, six bars, eight bars, ten bars, and twelve bars) on the spray properties by utilising a B20 blend of palm oil biofuel and diesel. According to the findings that they obtained, decreasing the droplet size of the fuel mixture lowered the rise in injection pressure as well as the emissions of CO and soot particles. Even at high pressures of injection, the concentration of nitrogen oxide (NO_x) emissions is less than the acceptable value, despite the fact that pressure of injection increases the amount of NO_x that is emitted.

In their research, Sung *et al.* [14] conducted a study on the impact of modifying the spray characteristics, particle size, and number distribution of moringa oleifera biofuel and its blends. This investigation was carried out using a common rail direct injection (CRDI) engine, with fuel injection pressures ranging from 300 to 600 bar and injection timings from 15.0 to 25.0 °CA before top dead center (TDC). Modifying the ranges of the two parameters. The injection timings were modified from 15.0 to 25.0 °CA before TDC. The use of higher injection pressure and earlier fuel injection led to a BTE of 33.49% for B20. The carbon monoxide emission of pure biodiesel was found to be at a minimum level of 0.01% volume, while the carbon dioxide (CO₂) emission reached a maximum level of 9.1% volume. Additionally, the emission of unburnt hydrocarbons was observed to be at a minimum level of 3 parts per million (ppm). In their study, Mehta *et al.* [15] conducted experiments on fuel blends consisting of waste cooking oil biodiesel (WOB), multi-walled carbon nanotubes (MWCNTs), aluminium oxide nanoparticles, and a base fuel. These experiments were carried out on a 5.2 kW CI engine, with a fixed rotational speed. The engine operated with a compression ratio of 17:1 and a fuel injection pressure of 175 bar. The nano-fuel composed of biodiesel which was produced from waste cooking oil (BWCO)/50 aluminium oxide nanoparticles (AONP)+50 MWCNT exhibited satisfactory performance. The BTE was measured to be 30.65%. The in-cylinder pressure was recorded at 58.36 bar, and the heat release rate was determined to be 38.38 J/CAD, with a minimum ignition delay (ID) of 9 CAD. The levels of NO_x emissions were found to be 954 ppm, while CO emissions were measured at 332 ppm. Additionally, the smoke opacity was observed to be 31.2% lower than the baseline measurement. Zhang *et al.* [16], Lajunen *et al.* [17], Sangwongwanich *et al.* [18] and Berruti *et al.* [19] conducted research on the impact of fuel mixtures containing waste vegetable oil blend (WOB) on engine performance parameters, including BTE, pressure, heat release rate, ignition delay, smoke emission, NO_x emissions, carbon monoxide (CO) emissions, and hydrocarbon (HC) emissions. The researchers made the observation that the use of the WOB combination resulted in enhanced performance characteristics, concurrently leading to a reduction in emissions emanating from the engine.

The works that have been reported on have shown both how dangerous plastic trash is and how it could be used in internal combustion (IC) engines. So, the present study suggested using 20% of waste plastics, 20% of waste cooking oil, and 20% of ethanol in an internal combustion engine with constant injection parameters (pressure and timing of injection, diameter of nozzle, and spray angle) and different engine loads. The new things about this study can be summed up as follows: i) the use of 20% of waste plastics (P20) prepared from waste plastics, ii) the use of 20% of waste cooking oil (W20) prepared from wastes oils, iii) the use of 20% of ethanol (E20), iv) investigates the properties of fuel mixture, and v) changes in engine loads to evaluate performance and environmental parameters and also test engine speed. Also, before P, W, and E in IC engine were looked into, it was tried to see what it was like. Rank the different engine settings using sensitivity analysis to see how well they work.

2. PRODUCTION OF WASTE PLASTIC OIL BIOFUEL AND TEST RING

2.1. Production of waste cooking oil biofuel

Palm oil, sunflower oil, mustard oil, and soya oil were chosen as the oils to compare and contrast in this inquiry because of the breadth of fatty acid profiles that each offers and the adaptability that each offers in the kitchen. There is a market in the city of Chidambaram, which is situated in the state of Tamil Nadu in India; here is where the oils were acquired. The manufacturing of biofuel required the use of alcohol as well as potassium hydroxide. Utilised cooking oils were melted down and utilised in the process. Through a chemical process known as transesterification as shown in Figure 1 is used cooking oils might be transformed into waste

cooking oil biofuel (also known as W) [20]–[24]. Before starting the process of transesterification, the W samples were filtered to remove any contaminants that could have been present. This was done so that the procedure could commence. Consideration of 20% ethanol and waste plastics oil biofuel, in addition to comparison to base fuel, is included in this research. Table 1 contains an overview of the various qualities of the fuel and fuel sample in Figure 2.

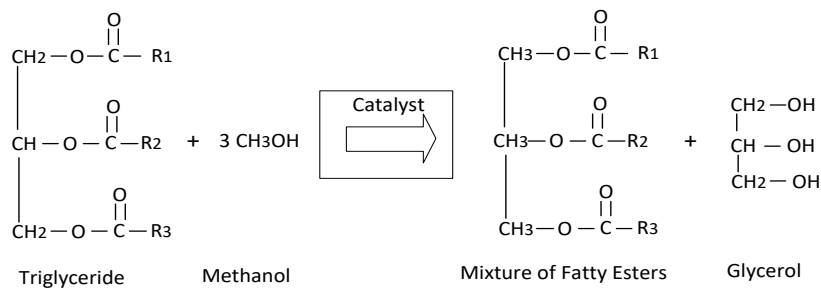


Figure 1. Transesterification



Figure 2. Sample of P20, W20 and E20

Table 1. The properties of blends

Property	Density (kg/m ³) at 15 °C	Flash point (°C)	Calorific value (MJ/kg)	Viscosity (mm ² /s) at 40 °C	Cetane number
BF100	838.0	61.2	45.5	3.8	45
W20	849.5	52.6	44.6	3.59	52.9
E20	824.1	-	40.49	2.45	49.4
P20	850	52.6	44.6	3.4	52.8

2.2. Experimental test ring

The manner in which the apparatus used in this investigation was assembled and arranged is seen in Figure 3. The engine subjected to rigorous testing was a diesel unit with a single cylinder, equipped with both direct injection and a common-rail injection system. Table 2 provides a comprehensive overview of the objectives and functioning of each engine. Table 3 presents a detailed overview of the many types of measurement equipment, their respective ranges, accuracies, techniques, and the corresponding percentages of error. The engine functions at its peak load and power output of 3.5 kW, while the common-rail injection technology it employs runs at a maximum injection pressure of 230 bar. Prior to any alterations, each test was conducted with the test engine in its initial condition. The engine of this test car meets the requirements of the Euro 4 emission standard with regards to its fuel pumping technology. The used test engine incorporates a pilot injection technique, a commonly utilised technology in diesel engines with indirect injection, aimed at mitigating the noise generated during the combustion process. The engine initiated pilot fuel injection (SOI) at a crank angle of 24.0 degrees before TDC. The first combustion pressure peak is expected to manifest in close proximity to the TDC and align with the pilot injection event. The shown waveform of the combustion pressure signal exhibits the occurrence of primary injection. In order to conduct this analysis, the full-load curve was used as a means to assess the precision of the engine's configuration. To get a comprehensive understanding of the influence of different fuel compositions on the operational characteristics of the engine, it is essential to conduct engine tests under conditions of maximum load. The reason for this phenomenon is that engines exhibit the highest fuel consumption while running at their maximum power output, also known as full load. Furthermore, it is worth noting that the engine's speed exhibits a fluctuation of 200 revolutions per minute

(rpm) within the range of 1,500 to 2,100 rpm. The selection of these three levels of engine speed at full load was based on their ability to effectively illustrate a wide range of the engine's operating capacities. In order to ascertain the torque and stopping power of the engine under full load conditions, an eddy current dynamometer was used. During this time frame, a gas analyzer was used to ascertain the volumes of different waste gases being breathed. The gas analyzers used in this study included the AVL as well as the engine gaseous emissions and smoke emissions, which were quantified using a smoke metre.

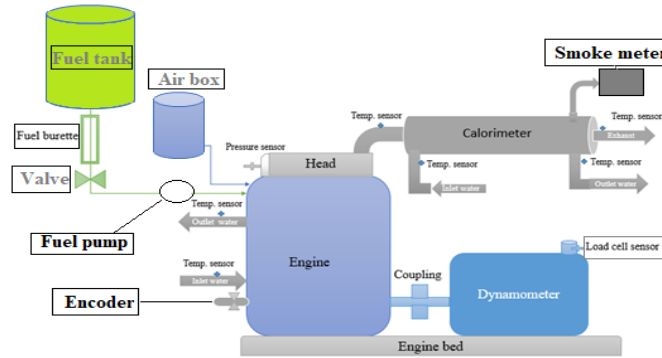


Figure 3. Test setup

Table 2. Provisions of assessment machine

Specification	Stroke/cylinder	Advanced FIP and IT	Rated power	Bore/stroke	Compression ratio
Limits	4/1	230 higher and 2.0 °b TDC	3.5 kW	80/110	19:1

2.3. Experimental error analysis

The findings of an uncertainty analysis are highly significant for scientific investigations since they inform the readers whether or not the data they were provided were accurate and whether or not they could be utilised again. Hence, the determination of the overall uncertainty value of the results is achieved by the application of the following (1) [25], [26] and the information that is shown in Table 3. The explanation of the markings may be found in the section of the book that is devoted to the names. A smoke metre was connected to the engine in order to measure the engine's gaseous emissions, and the smoke metre was used in order to measure the engine smoke releases. The equation states that the total amount of error that is conceivable is 2.36%.

$$\delta = [(\alpha_1)^2 + (\alpha_2)^2 + \dots + (\alpha_n)^2]^{1/2} \tag{1}$$

Table 3. Uncertainty

Apparatus	Uncertainty (%)
Encoder	±0.20
Fuel measurements	±1.0
Load cell	±0.20
CO2 emission	±1.0
NOx emission	±1.0
Pressure transducer	±0.50
Speed indicator	±1.0
Smoke	± 1.0
K-type (temperature)	±0.5

3. RESULTS AND DISCUSSION

3.1. Specific fuel consumption

Figure 4 illustrates the specific fuel consumption (SFC) figures corresponding to various injection timings during the operation of the engine under full load circumstances. When the engine was running under maximum load conditions, it was observed that the SFC values for W20 were comparatively greater than BF0 and P20, but lower than E20. The SFC values for BF0, E20, P20, and W20 were determined to be 0.26, 0.28,

0.262, and 0.273 kg/kWh, respectively, under 100% load operating conditions. Furthermore, when the injection time was adjusted at 23.5° b TDC, the SFC for W20 was found to be 4.7% higher than that of BF0. Due to its lower heating value in comparison to conventional fossil fuels, biodiesel need a greater quantity of fuel to provide an equivalent level of thermal energy. This contributes to an increase in the concentration of the SFC, which is classified as a greenhouse gas. The significance of the SFC is enhanced when there is an increased abundance of each constituent inside the amalgamation. The research demonstrates that an increase in load, coupled with appropriate ignition, results in a decrease in SFC concentration in comparison to diesel. This behaviour is not seen in the case of diesel fuel. Another contributing factor to the rise in SFC with higher percentages of biodiesel is the higher density of biodiesel fuel compared to petrol fuel [27], [28]. The increase in the SFC is seen when there exists a positive link between the proportion of biodiesel used and the quantity of biodiesel employed. The enhancement in fuel efficiency during full engine operation was attributed to the rise in temperature inside the cylinder, along with an augmentation in the quantity of oxygen present in the mixture [29].

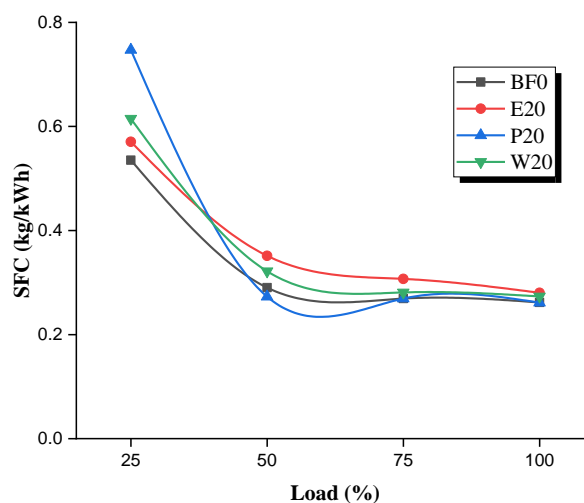


Figure 4. SFC with load

3.2. Brake thermal efficiency

Figure 5 shows BTE results for various injection times. BTE is the ratio of engine power to fuel energy pumped into the combustion chamber. The fuel's energy is calculated using its mass flow rate and lower heating value. The combustion cylinder had reduced fuel atomization, which improved BTE for biodiesel. Diesel is less viscous than biodiesel [30], which may explain this. Diesel is thinner than biodiesel. Blended fuels have a slightly lower BTE and higher BSFC than diesel fuel due to biodiesel's higher density and lower heating value. Because mixed fuels include more biodiesel [31], [32]. Figure 5 illustrates the BTE of the various petrol mixtures that were tested for a selection of different engine loads. The determination of the braking energy transfer efficiency, often referred to as the BTE, involves calculating the ratio between the braking power and the heat equivalent of the burned petrol. The aforementioned ratio is often referred to as the BTE, an acronym for "back to earth." The BTE for all fuel mixtures exhibited a lower average value compared to diesel fuel, perhaps due to the decreased energy content of the fuel blends. When doing a comparison between BF0, W20, P20, and E20 under full load conditions, it is seen that the BTE values for W20, P20, and E20 are lower by 2.1%, 4.2%, and 2.1% respectively, in comparison to BF0. This comparison is made at 100% load at an injection time of 23.5° b TDC. Both of these numbers have the same characteristics. The fuel combustion efficiency of the mixtures was enhanced during full load operation of the engine, owing to an increase in cylinder temperature and the concentration of oxygen in the intake. Consequently, it had a favourable impact on BTE and enhanced the efficiency of combustion. At elevated engine loads, the rise in in-cylinder temperature and the rate at which heat is released resulted in an increase in BTE ranging from 15.7% to 32.4% for BF0, 15.5% to 31.7% for E20, 16.5% to 31.1% for P20, and 14.1% to 31.78% for W20, across load conditions ranging from 25% to 100%.

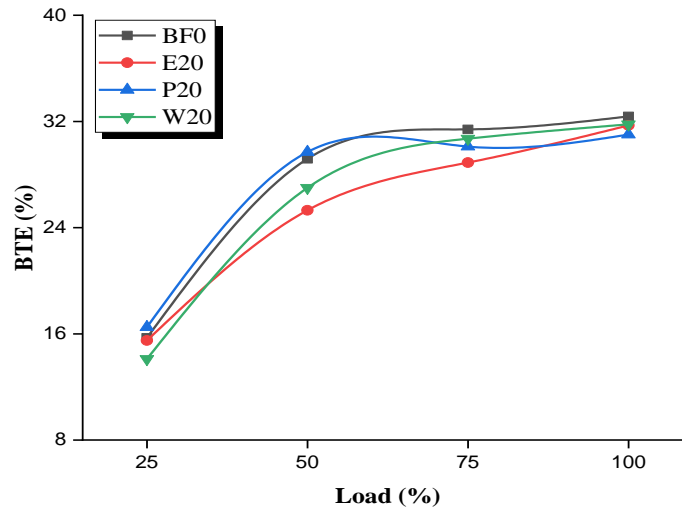


Figure 5. BTE with load

3.3. Cylinder pressure

Figure 6 depicts a graph of the cylinder pressure at the specified engine fuel-injection pump (FIP) for all of the fuels that were tested. The range of the curve is from 210 to 240 bar. Because of the high heat that is generated inside the cylinder, the cylinder peak pressure has a tendency to rise while the engine FIP rises. This is because of the relationship between the two variables. At 240 bar FIP, the peak pressure of W20, P20, and E20 reaches its highest value of 106, 86, and 119 bar, respectively. This is comparable to the peak pressure of diesel fuel (BF0), which is 122 bar at CR19 and 23.5 °b TDC when the fuel load condition is present. The surplus of oxygen sharing in W may be used to explain the increases in cylinder pressure that were seen in W20. An excessive amount of oxygen in the W at a low W share is what causes high cylinder and peak pressure during the diesel combustion process. This, in turn, has a negative impact on the engine's efficiency and the amount of emissions it produces. In point of fact, a greater CV often causes more wear and tear to be placed on the components of the engine [33]. The graphical representation in Figure 5 illustrates the correlation between crank angle and cylinder pressure for each of the experimental fuels. The aforementioned correlation can be seen for all of the experimental fuels. When the engine reached its maximum capacity, the BF100, W20, P20, and E20 all exhibited a consistent pressure pattern inside their individual cylinders. It is plausible that the engine's operation at maximum capacity may be attributed to the elevated viscosity of the fuel, its high latent heat of evaporation, and its suboptimal igniting properties [34], [35].

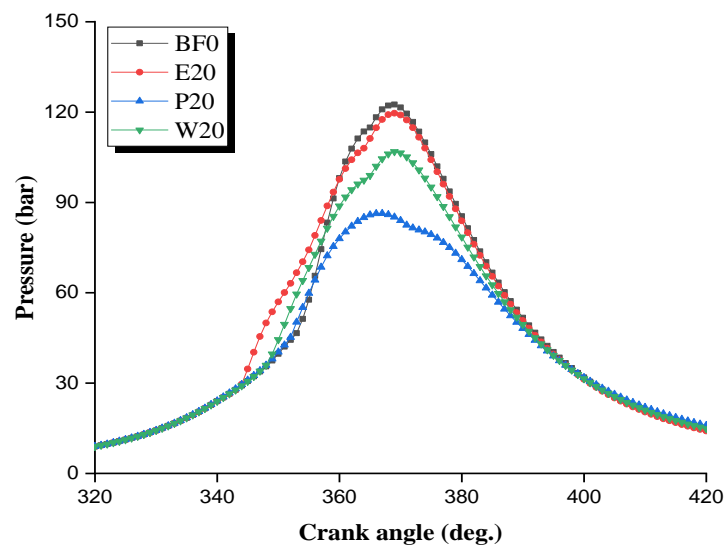


Figure 6. Cylinder pressure with crank angle

3.4. Ignition delay

Figure 7 depicts the ID of all the fuel samples at varying loads. The ID is shown for each of the test fuels in Figure 7, which may be found here. When the engines were filled to their full capacity, the ID readings all followed the same pattern. The graph shows that the engine ID drops as the load on the engine increases from 25% to 100%, and that the ID drops even more once E20, P20, and W20 are added. The E20 fuel has a somewhat lower heating value than P20, W20, and BF0, which results in a lower cylinder pressure and an even lower ID than those other fuels. When run at 1500 rpm, the BF0 reaches its maximum ID of 15.1 degrees, which is about 71%, 10.6%, and 39% higher than the E20, P20, and W20, respectively. The drop in the value of ID for mixes may be attributed to the fact that BF has a lower cetane number value than E20, P20, and W20 biofuel blends combined. Dong *et al.* [33] On the other hand, a greater cetane number indicates a shorter ignition delay, which indicates that there is less time for the air and fuel to combine before the premixed burning phase takes place. As a consequence of this, a weaker mixture would be formed and burnt during the period of premixed burning, which would result in a decrease in the production of NOx. Li *et al.* [36] there is a correlation between the chemical and physical qualities of the fuel and the igniting delay time. Because higher injection pressure results in better atomization properties, it may be possible to reduce the ignition delay by increasing the pressure. However, even though increasing the fraction of n-butanol enhances the atomization features, the ignition time is lengthened because of the larger cetane number. In addition to this, the ignition point might be found anywhere in the gasoline sprays farther downstream. Additionally, the ignition distance grows if either the injection pressure or the fraction of n-butanol rises.

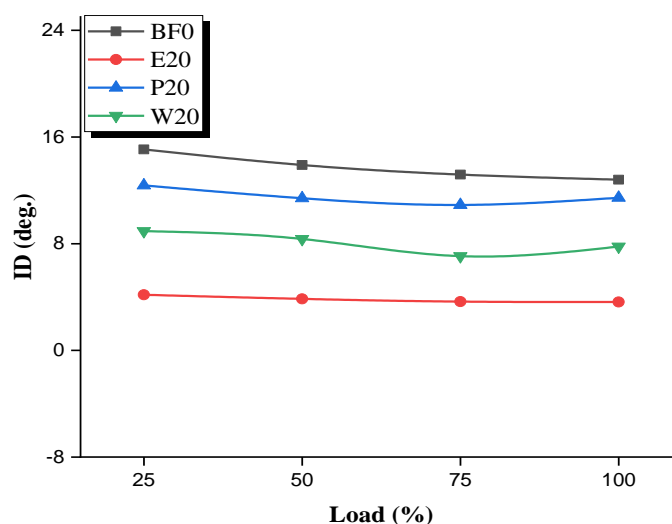


Figure 7. ID with load

3.5. Nitrogen oxides emission

Figure 8 shows the range of NOx emissions that can be made by changing the pumping time when using base fuel or biofuel. When the engines were running at full power with 1,500 rpm and CR19, the NOx emissions from BF0, E20, P20, and W20 all followed the same trend. BF0 has NOx levels of 217, 1,297, 3,036, and 3,372 ppm, while E20 has NOx levels of 644, 2,021, 3,265, and 3,630 ppm, for P20 has NOx levels of 163, 865, 1,262 and 2,031 ppm and W20 has NOx levels of 372, 1,627, 1,763, and 2,776 ppm with 25%, 50%, 75%, load 100% load respectively at 1,500 rpm and CR19. NOx are an emission product that should be avoided at all costs because of the danger it poses to humans and the environment. They are released during fuel combustion, in particular at high combustion temperatures. Nitric oxide, often known as NO, is the major component that contributes to the formation of NOx, along with a little amount of nitrogen dioxide (NO2) [33]. Pan *et al.* [37] observed that the rise in combustion temperature with the addition of hydrogen, as the combustion process in the CI engines happens at high oxygen levels, there may be a propensity for the NOx emissions to increase. One possible reason for this is that the temperature in the W is lower. When certain working conditions are met, like the air-to-fuel ratio, NOx emissions tend to go up as the combustion temperature goes up and the spark time moves the cetane number up [38]. There is a trend here that can be seen in some situations.

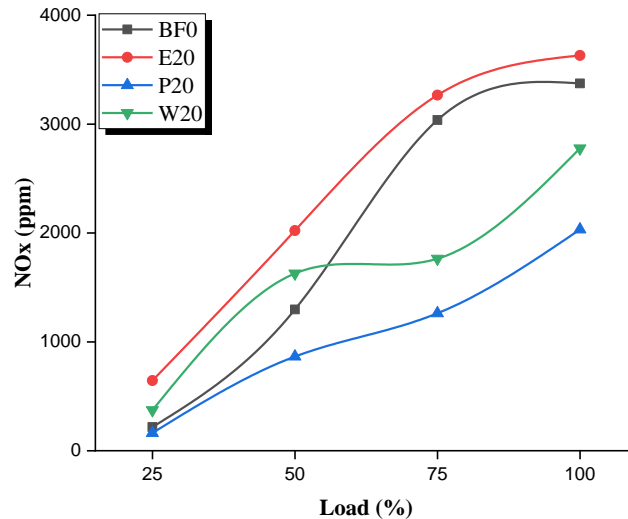


Figure 8. Engine NOx emission with loads

3.6. Smoke emission

By using fuels with high volatilities, it is feasible to effectively reduce the quantity of smoke discharged at early injection timings. The dominating factor in reducing smoke emissions via the use of fuel blends was the oxygenated content, particularly when the diesel energy ratio was increased. Conversely, the effect of fuel volatilities became more significant when the diesel energy ratio was decreased [39]. Both fuel composition and engine load were factors that led to the observed increase in smoke emissions from the engines. As the volume of entering fuel climbed in tandem with the augmented load, the provision of sufficient air became insufficient. Consequently, the quantity of smoke generated due to the enriched mixture likewise proportionally escalated [40], [41]. The range of hot soak loss (HSL) emissions obtained by altering the injection period for base fuel and biodiesel processes is shown in Figure 9. When the engines were filled to their utmost capacity, the smoke emission patterns generated by BF0, E20, P20, and W20 were indistinguishable. In comparison to the smoke emission levels of BF0 (11.8, 12.0, 17.2, and 36.9 HSL), the smoke emission levels of E20 (1.28, 1.2, 9.3, and 22.7 HSL), P20 (14.8, 17.62, 38.0, and 45.9 HSL), and W20 (10.1, 16.6, 20.7, and 43.1 HSL) were examined at 23.5 °b TDC and 25% to 100% load with CR19.

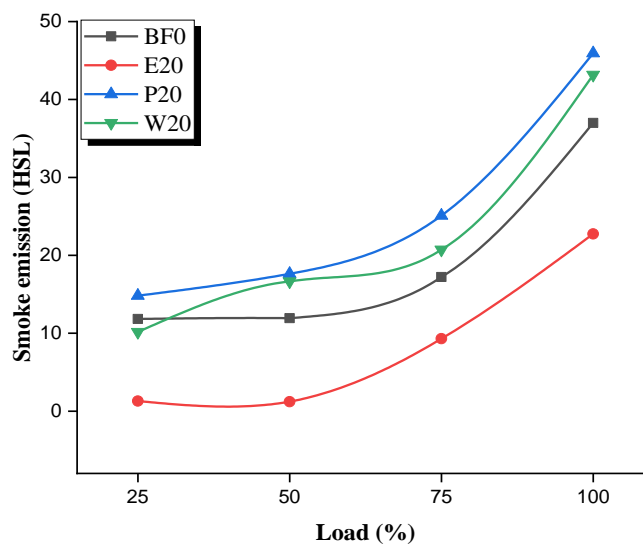


Figure 9. HSL emission with load

3.7. Carbon dioxide emission

According to Figure 10, the combination of E20 and BF0 produces the fewest amount of CO₂ emissions of any of the other options. Because biodiesel contains oxygen, carbon monoxide is transformed into carbon dioxide, and the fuel is burned to its full extent. The high cetane number in biodiesel blends is also responsible for the decreased formation in rich fuel, which was reported in [42]–[44]. The production of heat and the emission of carbon dioxide both stem from the incomplete combustion that had transpired. When comparing P20 to BF0, E20, and W20, the carbon dioxide emission from the P20 combination is greater by 24.0%. This is also true when comparing P20 to E20 and W20. PPO has a greater availability of oxygenated molecules, which is one of the reasons why its CO₂ emission is higher than diesel. This higher CO₂ emission results in enhanced combustion at higher loads and has a higher emission rate overall compared to diesel [45].

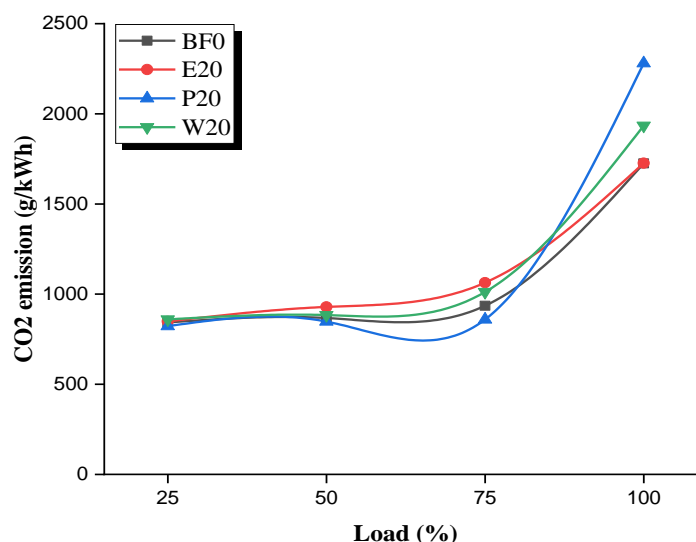


Figure 10. CO₂ emission with load

4. CONCLUSION

Provide densities and flash points of biodiesels produced with greater concentrations of W are well within the limits put forth by the specifications for biodiesel. When compared to the calorific value of base fuel, the calorific value of biodiesels made from waste oil is somewhat lower. This is due to the fact that waste oil may be used to create biodiesels. According to the findings of the engine research, BF0 has showed greater cylinder pressures in the same range as diesel in the combustion stage, but it has also shown a larger BTE in comparison to E20, P20, and W20 while having a lower SFC than E20, P20, and W20. When compared to the quantity that is decided by BF0, the value of BTE that is determined by W is much less than what is found to be the case. It has been discovered that the levels of NO_x generated by W20 and P20 at 23.5 °b TDC with 100% load are 17.6% and 39.7% lower, respectively, than the levels produced by BF0 with CR19. The maximum cylinder pressure of E20 (119.6 bar), P20 (86.3 bar), and W20 (106.8 bar) with 100% load is shown to be lowered by 2.3%, 41.9%, 12.8%, respectively, when compared to BF0 (122.5 bar). The results (P20 and W20) showed significantly greater levels of smoke emissions in comparison to the manufacture of BF0, whilst E20 showed much lower levels. When compared to the basic fuel, one may notice considerable variances in the quantity of NO_x emissions that are created. This may be the case since NO_x is a highly reactive gas.

REFERENCES





- [1] M. B. Kulkarni, U. S. Jayapiriya, K. Amreen, and S. Goel, "Portable thermal management platform for synthesis of ZnO nanoparticle in a microfluidic device: validated for electrochemical sensing and glucose fuel cell applications," *IEEE Transactions on Electron Devices*, vol. 68, no. 8, pp. 4070–4076, Aug. 2021, doi: 10.1109/TED.2021.3091954.
- [2] R. A. Farade *et al.*, "Investigation of the effect of sonication time on dispersion stability, dielectric properties, and heat transfer of graphene based green nanofluids," *IEEE Access*, vol. 9, pp. 50607–50623, 2021, doi: 10.1109/ACCESS.2021.3069282.
- [3] A. Tavakoli, A. Karimi, and M. Shafie-Khah, "Linearized stochastic optimization framework for day-ahead scheduling of a biogas-based energy hub under uncertainty," *IEEE Access*, vol. 9, pp. 136045–136059, 2021, doi: 10.1109/ACCESS.2021.3116028.
- [4] F. Rojas-Perez, J. A. Castillo-Benavides, G. Richmond-Navarro, and E. Zamora, "CFD modeling of plasma gasification reactor for municipal solid waste," *IEEE Transactions on Plasma Science*, vol. 46, no. 7, pp. 2435–2444, Jul. 2018, doi: 10.1109/TPS.2018.2844867.

- [5] M. J. A. R. Rivas, D. Capuano, and C. Miranda, "Economic and environmental performance of biowaste-to-energy technologies for small-scale electricity generation," *Journal of Modern Power Systems and Clean Energy*, vol. 10, no. 1, pp. 12–18, 2022, doi: 10.35833/MPCE.2020.000315.
- [6] M. P. Wilson *et al.*, "Impulse-breakdown characteristics of polymers immersed in insulating oil," *IEEE Transactions on Plasma Science*, vol. 38, no. 10, pp. 2611–2619, Oct. 2010, doi: 10.1109/TPS.2010.2044877.
- [7] C. Ottesen *et al.*, "Compatibility of printed photopolymers with nine-month immersion in common high voltage insulation oils," *IEEE Transactions on Plasma Science*, vol. 48, no. 10, pp. 3312–3320, Oct. 2020, doi: 10.1109/TPS.2020.2978203.
- [8] Y. Lee *et al.*, "Removal of mist particles by a two-stage electrostatic precipitator featuring plastic plate electrodes," *IEEE Transactions on Industry Applications*, vol. 58, no. 3, pp. 3985–3991, May 2022, doi: 10.1109/TIA.2022.3159306.
- [9] M. P. Wilson *et al.*, "Effect of applied field and rate of voltage rise on surface breakdown of oil-immersed polymers," *IEEE Transactions on Dielectrics and Electrical Insulation*, vol. 18, no. 4, pp. 1003–1010, Aug. 2011, doi: 10.1109/TDEI.2011.5976088.
- [10] G. Wang and Y. Zhou, "Thermal management modeling for β -Ga₂O₃-highly thermal conductive substrates heterostructures," *IEEE Transactions on Components, Packaging and Manufacturing Technology*, vol. 12, no. 4, pp. 638–646, Apr. 2022, doi: 10.1109/TCPMT.2022.3157672.
- [11] M. Chen, H. Wang, D. Pan, X. Wang, and F. Blaabjerg, "Thermal characterization of silicon carbide MOSFET module suitable for high-temperature computationally efficient thermal-profile prediction," *IEEE Journal of Emerging and Selected Topics in Power Electronics*, vol. 9, no. 4, pp. 3947–3958, Aug. 2021, doi: 10.1109/JESTPE.2020.2984586.
- [12] X. Han, Q. Cheng, F. Liu, and Y. Yu, "Numerical analysis on thermal tuning efficiency and thermal stress of a thermally tunable SG-DBR laser," *IEEE Photonics Journal*, vol. 8, no. 3, pp. 1–12, Jun. 2016, doi: 10.1109/JPHOT.2016.2558042.
- [13] Y. Wang, P. Liu, D. Liu, F. Deng, and Z. Chen, "Enhanced hierarchical control framework of microgrids with efficiency improvement and thermal management," *IEEE Transactions on Energy Conversion*, vol. 36, no. 1, pp. 11–22, Mar. 2021, doi: 10.1109/TEC.2020.3002670.
- [14] Y.-M. Sung, Y.-C. Huang, F. S.-S. Chien, and C.-S. Tsao, "Mechanism and analysis of thermal burn-in degradation of OPVs induced by evaporated HTL," *IEEE Journal of Photovoltaics*, vol. 9, no. 3, pp. 694–699, May 2019, doi: 10.1109/JPHOTOV.2019.2894765.
- [15] K. Mehta *et al.*, "Thermal design considerations for III-N vertical-cavity surface-emitting lasers using electro-opto-thermal numerical simulations," *IEEE Journal of Quantum Electronics*, vol. 55, no. 5, pp. 1–8, Oct. 2019, doi: 10.1109/JQE.2019.2937991.
- [16] C. Zhang, J. Liu, R. Sun, C.-P. Wong, L. Ren, and X. Zeng, "Effects of in situ modification of aluminum fillers on the rheological properties and thermal resistance of gel thermal interface materials," *IEEE Transactions on Components, Packaging and Manufacturing Technology*, vol. 12, no. 8, pp. 1302–1310, Aug. 2022, doi: 10.1109/TCPMT.2022.3192023.
- [17] A. Lajunen, Y. Yang, and A. Emadi, "Review of cabin thermal management for electrified passenger vehicles," *IEEE Transactions on Vehicular Technology*, vol. 69, no. 6, pp. 6025–6040, Jun. 2020, doi: 10.1109/TVT.2020.2988468.
- [18] A. Sangwongwanich, H. Wang, and F. Blaabjerg, "Reduced-order thermal modeling for photovoltaic inverters considering mission profile dynamics," *IEEE Open Journal of Power Electronics*, vol. 1, pp. 407–419, 2020, doi: 10.1109/OJPEL.2020.3025632.
- [19] G. M. Berruti *et al.*, "Highly efficient fiber optic thermal heating device based on turn-around-point long period gratings," *Journal of Lightwave Technology*, vol. 40, no. 3, pp. 797–804, Feb. 2022, doi: 10.1109/JLT.2021.3121775.
- [20] T. Qi and S. He, "Further efficiency improvement of power amplifiers using thermal energy harvesting," *IEEE Transactions on Industrial Electronics*, vol. 66, no. 12, pp. 9628–9631, Dec. 2019, doi: 10.1109/TIE.2018.2885742.
- [21] L. Xu *et al.*, "Accurate and efficient thermal analysis of slow wave structures for helix traveling-wave tubes by finite-element method," *IEEE Transactions on Electron Devices*, vol. 68, no. 4, pp. 1905–1911, Apr. 2021, doi: 10.1109/TEDE.2021.3059179.
- [22] B. Han *et al.*, "Investigation on thermal efficiency enhancement and sideband emission suppression for magnetron injection gun," *IEEE Transactions on Electron Devices*, vol. 70, no. 4, pp. 1923–1928, Apr. 2023, doi: 10.1109/TEDE.2023.3246027.
- [23] L. Rui *et al.*, "Electron gun thermal depended properties" analysis of a high-power W-band sheet beam extended oscillator," *IEEE Transactions on Electron Devices*, vol. 67, no. 2, pp. 684–689, Feb. 2020, doi: 10.1109/TEDE.2019.2958994.
- [24] J. Qi, W. Hua, and H. Zhang, "Thermal analysis of modular-spoke-type permanent-magnet machines based on thermal network and FEA method," *IEEE Transactions on Magnetics*, vol. 55, no. 7, pp. 1–5, Jul. 2019, doi: 10.1109/TMAG.2019.2905873.
- [25] V. Gahlaut, A. M. Latha, R. K. Sharma, and S. K. Ghosh, "Thermal management techniques for novel single-stage collector of THz folded waveguide TWT," *IEEE Transactions on Plasma Science*, vol. 49, no. 2, pp. 689–694, Feb. 2021, doi: 10.1109/TPS.2020.3047423.
- [26] M. Ghiyasi, B. D. Rouyendegh, and Y. S. Ozdemir, "Local and global energy efficiency analysis for energy production based on multi-plant generalized production technology," *IEEE Access*, vol. 9, pp. 58208–58215, 2021, doi: 10.1109/ACCESS.2021.3072493.
- [27] M. Mahrokh, H. Yu, and Y. Guo, "Thermal modeling of GaN HEMT devices with diamond heat-spreader," *IEEE Journal of the Electron Devices Society*, vol. 8, pp. 986–991, 2020, doi: 10.1109/JEDS.2020.3023081.
- [28] R. Burke, A. Giedymin, Z. Wu, H. Chuan, N. Bourne, and J. G. Hawley, "A lumped parameter thermal model for single-sided AFPM machines with experimental validation," *IEEE Transactions on Transportation Electrification*, vol. 6, no. 3, pp. 1065–1083, Sep. 2020, doi: 10.1109/TTE.2020.2998110.
- [29] Z. Wang, G. Ehrke, B. Mendelevitch, J. Boscary, and R. Stadler, "Thermal and mechanical analysis of the wendelstein7-X cryo-vacuum pump plug-in," *IEEE Transactions on Plasma Science*, vol. 46, no. 5, pp. 1576–1579, May 2018, doi: 10.1109/TPS.2017.2763152.
- [30] W. Zhu, G. Dong, and Y. Yang, "Thermal-aware modeling and analysis for a power distribution network including through-siliconvias in 3-D ICs," *IEEE Transactions on Computer-Aided Design of Integrated Circuits and Systems*, vol. 38, no. 7, pp. 1278–1290, Jul. 2019, doi: 10.1109/TCAD.2018.2846659.
- [31] P.-H. Lee, W.-M. Tu, and H.-C. Tseng, "Graphene heat spreaders for thermal management of InGaP/GaAs collector-up HBTs," *IEEE Transactions on Electron Devices*, vol. 65, no. 1, pp. 352–355, Jan. 2018, doi: 10.1109/TEDE.2017.2762360.
- [32] D. Li, H. Zhang, and Y. Sun, "A CO₂ gas thermal conductivity sensor based on GO/ α -Al₂O₃ functional material," *IEEE Sensors Journal*, vol. 21, no. 14, pp. 15952–15961, Jul. 2021, doi: 10.1109/JSEN.2021.3061565.
- [33] T. Dong, C. Zhu, F. Zhou, H. Zhang, F. Lu, and X. Zhang, "Innovated approach of predictive thermal management for high-speed propulsion electric machines in more electric aircraft," *IEEE Transactions on Transportation Electrification*, vol. 6, no. 4, pp. 1551–1561, Dec. 2020, doi: 10.1109/TTE.2020.3017764.
- [34] A. A. Hawwash, M. Ahamed, S. A. Nada, A. Radwan, and A. K. Abdel-Rahman, "Thermal analysis of flat plate solar collector using different nanofluids and nanoparticles percentages," *IEEE Access*, vol. 9, pp. 52053–52066, 2021, doi: 10.1109/ACCESS.2021.3060004.
- [35] H. Fu, J. Chen, A. S. Bahman, R. Qiu, and Z. Liu, "An online identification method of thermal dissipation state for forced air-cooled system of power converters," *IEEE Journal of Emerging and Selected Topics in Power Electronics*, vol. 10, no. 6, pp. 7677–7690, Dec. 2022, doi: 10.1109/JESTPE.2022.3186178.





- [36] Z. Li, J. Zheng, J. Li, W. Zhan, and Y. Chen, "Enhanced optical and thermal performance of QD white LEDs using a centrifugation packaging structure," *IEEE Photonics Technology Letters*, vol. 33, no. 14, pp. 727–730, Jul. 2021, doi: 10.1109/LPT.2021.3090058.
- [37] G. Pan, M. Xun, Z. Zhao, Y. Sun, J. Zhou, and D. Wu, "High slope efficiency bipolar cascade 905nm vertical cavity surface emitting laser," *IEEE Electron Device Letters*, vol. 42, no. 9, pp. 1342–1345, Sep. 2021, doi: 10.1109/LED.2021.3098899.
- [38] X. Yi, T. Yang, J. Xiao, N. Miljkovic, W. P. King, and K. S. Haran, "Equivalent thermal conductivity prediction of form-wound windings with litz wire including transposition effects," *IEEE Transactions on Industry Applications*, vol. 57, no. 2, pp. 1440–1449, Mar. 2021, doi: 10.1109/TIA.2021.3053500.
- [39] C. Zhang, Y. Xu, Z. Li, and Z. Y. Dong, "Robustly coordinated operation of a multi-energy microgrid with flexible electric and thermal loads," *IEEE Transactions on Smart Grid*, vol. 10, no. 3, pp. 2765–2775, May 2019, doi: 10.1109/TSG.2018.2810247.
- [40] J. Zhang, Z. Zhang, Y. Xia, and L. Yu, "Thermal analysis and management for doubly salient brushless DC generator with flat wire winding," *IEEE Transactions on Energy Conversion*, vol. 35, no. 2, pp. 1110–1119, Jun. 2020, doi: 10.1109/TEC.2020.2966046.
- [41] S. H. Shah, X. Wang, M. Azeem, and U. Abubakar, "Coupled magnetic field and thermal analysis model for an ipmsm with modular three-phase winding topologies for fault-tolerant applications," *IEEE Access*, vol. 10, pp. 30335–30348, 2022, doi: 10.1109/ACCESS.2022.3158672.
- [42] A. M. Latha, V. Gahlaut, R. K. Sharma, V. Srivastava, and S. K. Ghosh, "Multistage depressed collector with improved thermal management for high efficiency travelling wave tubes," *IEEE Transactions on Electron Devices*, vol. 61, no. 5, pp. 1536–1540, May 2014, doi: 10.1109/TED.2014.2309339.
- [43] D. Jin *et al.*, "Thermal design of VCSEL arrays for optical output power improvement," *IEEE Transactions on Electron Devices*, vol. 69, no. 7, pp. 3761–3767, Jul. 2022, doi: 10.1109/TED.2022.3177164.
- [44] D. Coenen *et al.*, "Thermal modelling of silicon photonic ring modulator with substrate undercut," *Journal of Lightwave Technology*, vol. 40, no. 13, pp. 4357–4363, Jul. 2022, doi: 10.1109/JLT.2022.3162987.
- [45] K. Zeng and D. Jiao, "Matrix-free method for transient maxwell-thermal cosimulation in arbitrary unstructured meshes," *IEEE Transactions on Microwave Theory and Techniques*, vol. 66, no. 12, pp. 5439–5448, Dec. 2018, doi: 10.1109/TMTT.2018.2875105.

BIOGRAPHIES OF AUTHORS



D.V.S.R.B.M. Subrahmanyam     has successfully obtained a bachelor of technology degree in mechanical engineering from Bundelkhand University, Jhansi, and a master of engineering degree in machine design from Rajeev Gandhi Technical University, Bhopal. Currently, he is actively engaged in the pursuit of a doctor of philosophy degree in the field of mechanical engineering at Annamalai University, located in Chidambaram. The focus of his study is on the enhancement of thermal engineering and design. He can be contacted at email: subhramanyasharma@gmail.com.



Dr. Manikandan Jegathesan     has successfully obtained a bachelor of engineering degree in mechanical engineering, a master of engineering degree in energy engineering and management, and a doctor of philosophy degree in mechanical engineering from Annamalai University, located in Chidambaram, Tamil Nadu state, India. He has been actively engaged in technological research for over twenty years. The individual in question has authored over ten research articles in esteemed academic publications, focusing on the field of mechanical engineering and its corresponding Ph.D. candidates. Currently, he is assigned to the Constituent College of Anna University. He can be contacted at email: jmanikandanrishi@rediffmail.com.